energy&fuels

Article

Cite This: Energy Fuels 2018, 32, 4300−4307

pubs.acs.org/EF

Particle Size Distributions of Fly Ash Arising from Vaporized Components of Coal Combustion: A Comparison of Theory and Experiment

Huimin Liu,[†] Yueming Wang,[‡] and Jost O. L. Wendt*[,‡]

[†]School of Energy, Power and Mechanical Engineering, North China Electric Power University, Baoding, Hebei 071003, People's Republic of China

[‡]Department of Chemical Engineering and Institute for Clean and Secure Energy, University of Utah, Salt Lake City, Utah 84124, United States

Supporting Information

ABSTRACT: A 100-kW-rated down-fired pilot-scale combustor was used to explore sub-micrometer coal ash aerosol formation for two coals under various air and oxy-combustion atmospheres. Particle size distribution (PSD) data were obtained through isokinetic sampling and then by electron mobility and light-scattering particle sizing. The sub-micrometer portion of the PSD exhibited an "accumulation" mode at ∼0.3 μm and, in some cases, an additional "nucleation" mode between 0.03 and 0.07 μm. Predictions of the temporal evolution of the sub-micrometer aerosol were made using a sectional coagulation model. A comparison to experimental measurements suggested that the "accumulation" mode was formed by coagulation of vaporized silicon-rich species, which occurred and was completed very close to the parent char particle and not in the mixed flue gas. This showed the importance of carefully characterizing microscale mixing phenomena around individual particles. For the sodium-rich species that had heretofore been thought to nucleate in the sampling probe, it now seems that they nucleate within the furnace, but coagulation without particle growth was insufficient to explain the location of the "nucleation" modes for all but one case explored. For that one coal, the "nucleation" mode was dominated by high concentrations of particles containing calcium, and there, its location was consistent with coagulation. Additional modeling involving both coagulation and particle growth is required.

1. INTRODUCTION

Particulate matter (PM), emitted from coal combustion, can be a major source of atmospheric PM pollution. In comparison to super-micrometer particles (>1 μm), sub-micrometer particles (<1 μm) can cause more serious harm to human health as a result of their long residence times in the air and their much lower capture efficiencies by electrostatic precipitators (ESPs), with only 85−95% for PM_1 and 95−99% for $PM_{2.5}$ compared to the up to 99.9% efficiency for PM_{10+} ash particles.[1,2] Furthermore, these sub-micrometer particles are enriched in hazardous trace elements, such as cadmium and arsenic.[3−5]

There is a vast body of literature on particle size distributions (PSDs) and formation mechanisms of ash particles from coal combustion.[6−11] The consistent result is that the ash PSD contains several modes.[12] Those modes lying below ∼0.6 μm have been designated "vaporization" modes, because they are formed by ash constituents that vaporized in the hot part of the flame and subsequently nucleated and coagulated in both the furnace and possibly the cooled, dilution sample probe that was used to collect them. The modes greater than ∼0.6 μm are designated "fragmentation" modes, because they result from ash particles that are released during the coal char oxidation portion of the coal combustion process. In this work, we focus only on the vaporization modes.

Two modes in the <0.6 μm domain have been observed in previous studies,[10,13,14] with one below 0.1 μm, often designated as a "nucleation" mode, the other lying at ∼0.3 μm and designated as an "accumulation" mode. It has been hypothesized previously that nucleation modes represent particles formed by nucleation/coagulation of vaporized species inside the sampling probe, while the accumulation mode was formed by nucleation and subsequent coagulation of vaporized species within the furnace.[10] Researchers at Massachusetts Institute of Technology (MIT)[15,16] introduced a mechanism whereby sub-micrometer refractory species, such as SiO_2, were formed from mineral matter in burning char. Si is chemically reduced to form volatile suboxide vapors that diffuse through fuel-rich regions until they meet oxygen at the flame front, where they are quickly oxidized into refractory SiO_2 that nucleates and coagulates. The process to form nucleated SiO_2 occurs close to the particle, but the domain (near the particle or dispersed in the furnace) in which coagulation of these nuclei occurs has not been determined. An objective of this work was to make quantitative comparisons between measured and predicted sub-micrometer PSDs of coal ash obtained in a down-fired laboratory coal combustor that had particle concentrations and temperatures similar to practical units. Furthermore, we demonstrate how these predictions can provide insight into the

Special Issue: 6th Sino-Australian Symposium on Advanced Coal and Biomass Utilisation Technologies

Received: October 13, 2017
Revised: November 15, 2017
Published: November 17, 2017

DOI: 10.1021/acs.energyfuels.7b03126
Energy Fuels 2018, 32, 4300−4307

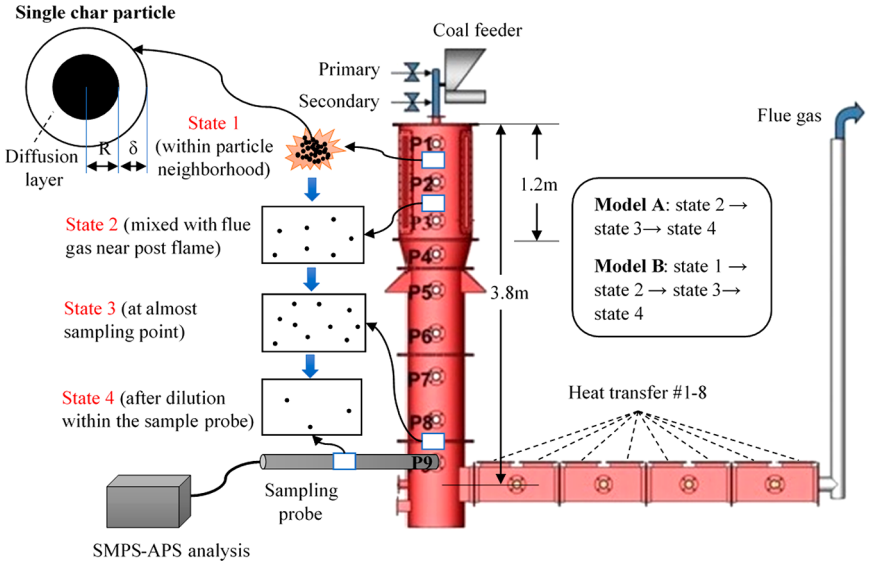

Figure 1. 100-kW-rated down-fired pilot-scale combustor.

Table 1. Ultimate and Proximate Analyses of Coals (As-Received Basis)

	ash (%)	C (%)	H (%)	N (%)	S (%)	O[a] (%)	moisture (%)	volatile (%)	fixed carbon (%)	HHV[b] (BTU/lb)
PRB	4.94	53.72	6.22	0.78	0.23	34.11	23.69	33.36	38.01	9078
Utah	8.36	67.87	5.45	1.09	0.36	16.87	6.11	38.49	47.04	11899

[a]Obtained by difference [b]Higher heat value.

Table 2. Ash Composition of Coals

	Al_2O_3 (%)	CaO (%)	Fe_2O_3 (%)	MgO (%)	MnO (%)	P_2O_5 (%)	K_2O (%)	SiO_2 (%)	Na_2O (%)	SO_3 (%)	TiO_2 (%)
PRB	14.78	22.19	5.2	5.17	0.01	1.07	0.35	30.46	1.94	8.83	1.3
Utah	8.34	18.21	5.25	2.84	0.05	0.01	0.33	48.85	3.09	5.96	0.64

domain over which coagulation occurs and, thus, aid in the future development of simulations of ash partitioning.

It would be convenient if furnace simulations were not compelled to model detailed events caused by microscale diffusion phenomena within the neighborhood of each particle, and few simulation programs do so. Microscale diffusion phenomena during coal combustion are known to affect volatile coal nitrogen conversion to NO, even for totally "premixed" coal air flames.[17] There are also diffusion layers around burning char particles, and these have been modeled by computer codes, such as SKIPPY.[18−20] In this paper, we address the question of where and how should one model the coagulation process resulting from vaporized ash mineral matter. For example, one can pose the question: Is this process completed within the diffusion layer surrounding a burning char particle or did it spread throughout the flue gas in the furnace?

2. EXPERIMENT

A 100-kW-rated down-fired pilot-scale combustor was used to measure ash aerosols of two typical coals [Utah Sufco coal and Powder River Basin (PRB) coal] under various air and oxy-combustion atmospheres. The combustor is shown in Figure 1. Detailed descriptions on the combustor and particle sampling system can be found elsewhere.[10,21]

The ultimate and proximate analyses and ash composition of coal samples are shown in Tables 1 and 2, respectively.

Combustion parameters under different atmospheres are listed in Table 3. A total of five cases was considered, including air and oxy atmospheres with various inlet oxygen concentrations (27% inlet O_2 as OXY27, 50% inlet O_2 as OXY50, and 70% inlet O_2 as OXY70).

Table 3. Combustion Parameters

	Utah coal			PRB coal	
	OXY27	OXY70	air	OXY27	OXY50
coal feed rate (kg/h)	3.46	3.46	4.54	4.54	4.54
particle density (kg/m^3)	1300	1300	1200	1200	1200
adiabatic flame temperature (K)	2000	2900	2000	2000	2600
gas flow rate at 300 K (m^3/h)	22.41	8.96	30.65	23.59	13.36

Ash aerosols from these cases were sampled through port 9 (see Figure 1) using an isokinetic dilution probe.[21] With electron mobility [scanning mobility particle sizer (SMPS)] and light scattering [aerodynamic particle sizer (APS)] technology, the PSDs of ash aerosols under various atmospheres are shown in Figure 2.

Figure 2 shows all of the modes of ash particles in the range of 0.014−20 μm, including both "vaporization" and "fragmentation" modes. In this work, only the vaporization modes under 1 μm are discussed. Despite the differences in coal properties and combustion atmospheres, two vaporization modes were observed in Figure 2, with the nucleation mode under 0.1 μm and the accumulation mode near 0.3 μm. It was hypothesized that both modes were formed by nucleation/coagulation, with the former mode inside the sample probe and the latter mode in the furnace that has heretofore not been validated. In the sections below, a model based on the coagulation theory was applied and compared to the experimental data, with the objective to reveal where and how the two vaporization modes formed in the post-combustion process.

DOI: 10.1021/acs.energyfuels.7b03126
Energy Fuels 2018, 32, 4300−4307

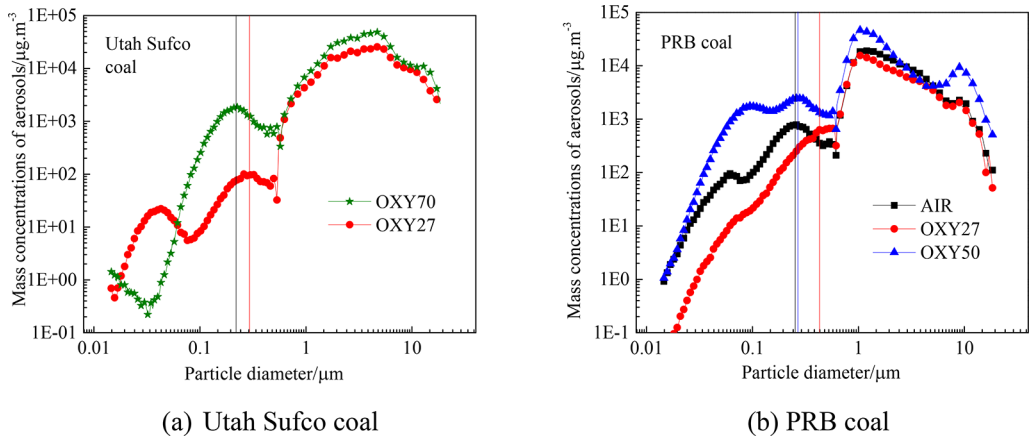

Figure 2. Mass concentration of size-segregated ash particles.[22]

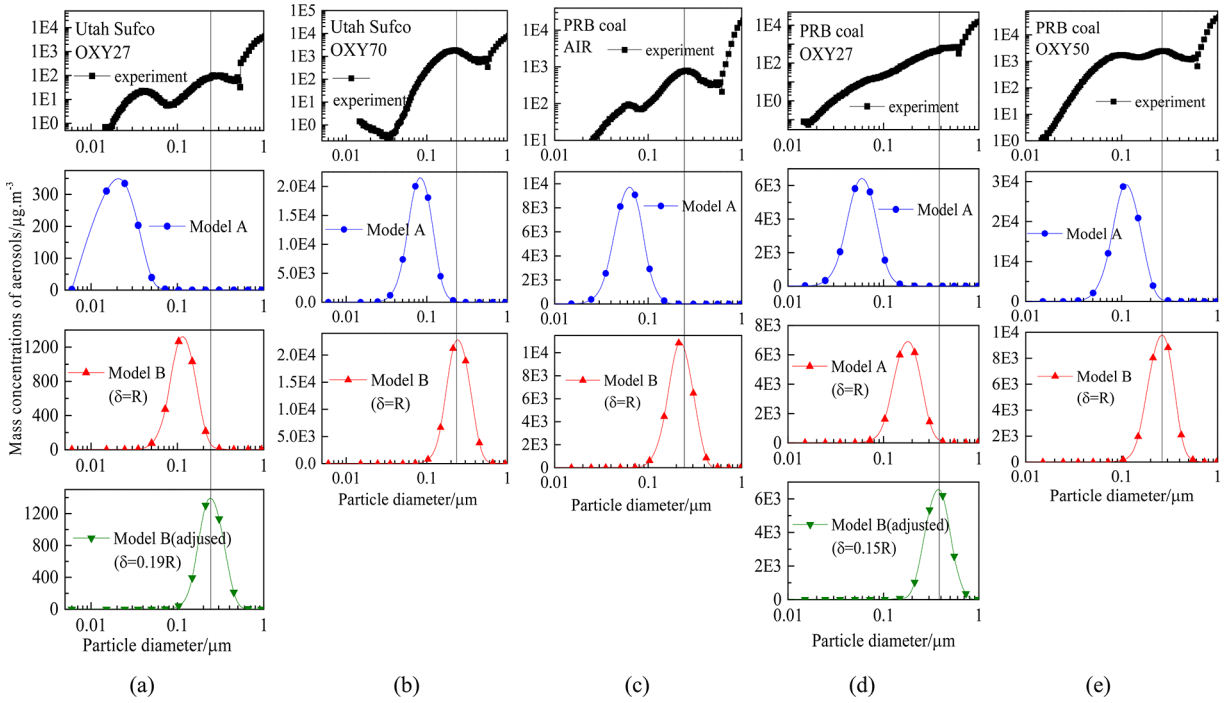

Figure 3. Comparison of predicted and experimental accumulation modes.

3. MODEL

Model predictions were carried out using a multicomponent aerosol simulation code (MAEROS),[23] which was first described by Gelbard and Seinfeld. It is a useful tool to predict the aerosol mass concentration of an arbitrary number of chemical components for an arbitrary number of particle-size classes, called sections. With an initial aerosol mass concentration in each section as input, the code integrates the discretized version of the general dynamic equation (GDE) for aerosols to predict the temporal evolution of the chemical component mass concentration distribution.[24] The same theoretical model and computational methods were also validated and verified by Gelbard et al.[25] in their simulation of aerosol dynamics in the marine boundary layer. This code has been applied to combustion environments, and the accuracy is reliable.[26−29] As far as the "vaporization" modes are concerned, only the coagulation subroutine of MAEROS was used for the predictions in this paper. Because leakage of aerosols as a result of deposition was not considered in this study, the MAEROS code was modified to allow for changes in gas specific volume during the calculation process based on conservation of aerosol mass.

3.1. Model Input. The mass of ash vaporized to form the observed accumulation/nucleation mode was taken from the experimental data. Through integration of the area under the accumulation/nucleation mode, the total mass of vaporized ash aerosol was obtained, and this was all put into the first section (or particle bin). Differences in the temperature in the sample volume (data) and in the furnace (prediction) were taken into account. The first section size is set at 2−10 nm, which represents a reasonable initial size of aerosol nuclei. Additional runs exploring the effect of nuclei diameter, within the range of 10−20 nm, showed that, at a constant nuclei mass, the effect of the nuclei diameter was extremely small, as was expected. For all of the other sections with larger particle sizes, the initial input was zero.

In addition, it is noted that, in the MAEROS code, the difference of gas compositions in the five cases considered is manifested mainly by two specific parameters: the molecular weight of the flue gas and the gas temperature (history), because they determine the density and viscosity of gas and, thus, affect the collision coefficient of particles and final PSDs.

Detailed input parameters of MAEROS used to predict the accumulation modes for the five cases investigated here are listed in Tables S1−S5 of the Supporting Information. This has been added to

DOI: 10.1021/acs.energyfuels.7b03126
Energy Fuels 2018, 32, 4300−4307

Table 4. Parameters for Accumulation Mode Prediction with Model A

accumulation mode with model A	Utah coal		PRB coal		
	OXY27	OXY70	air	OXY27	OXY50
total mass of vaporized ash for prediction (kg/h)	6.92×10^{-5}	4.62×10^{-4}	7.15×10^{-4}	3.66×10^{-4}	9.10×10^{-4}
initial temperature at state 2, T2 (K)	2000	2900	2000	2000	2600
initial gas volume at state 2, V2 (m^3/h)	149.40	86.61	204.33	157.27	115.79
initial mass concentration of particles, C2 (kg/m^3)	4.63×10^{-7}	5.34×10^{-6}	3.50×10^{-6}	2.33×10^{-6}	7.86×10^{-6}
temperature at state 3, T3 (K)	1038	960	1062	1082	961
residence time in the furnace from state 2 to state 3, t_{23} (s)	7	16	12	16	26
residence time in the probe from state 3 to state 4, t_{34} (s)	0.25	0.25	0.25	0.25	0.25
predicted peak diameter (μm)	0.02	0.09	0.07	0.06	0.11
experimental peak diameter (μm)	0.30	0.22	0.24	0.38	0.29

this paper to allow for other researchers to test their models against the same input data. For the nucleation mode input, please see Tables S6–S9 of the Supporting Information (note that no nucleation mode occurred for Utah Sufco OXY70). It is hoped that sufficient detail is provided throughout this paper, including the Supporting Information, so that others can repeat these calculations using different models and different computer simulations.

4. RESULTS AND DISCUSSION

Results consist of comparisons between predictions of the PSDs and the experimental measurements. They are presented in two sections. In the first section (section 4.1), attention is focused on the prediction of the location of the accumulation mode. To simulate the data, three reactor model configurations were explored. Model A, which was attempted first, used a conventional approach, in which all of the particles coagulate in the mixed flue gas until they were sampled. This model could not be made to agree with the data. Consequently, model B was developed, and this assumed that coagulation occurred primarily within a diffusion layer surrounding each burning coal/char particle, where the diffusion layer was one particle radius out from each particle. After a short time, 0.05 s, the particles mixed with the flue gas as in model A. Where this also fell short of the measurements, model B (adjusted) was introduced, where the thickness of the diffusion layer was adjusted to determine whether any reasonable reactor configuration might explain the data through coagulation alone.

In the second section (section 4.2), attention is focused on the location of the nucleation mode (where it exists), and again, attempts were made to predict its location using coagulation mechanisms alone. These comparisons were of limited success, and the consequences of that in terms of mechanisms are discussed together with the results.

4.1. Accumulation Mode. Predictions of the fly ash aerosol accumulation mode for the five cases investigated (Table 3) are shown in Figure 3 and compared to the experimental data depicted on the top panel of each of the five subgraphs. The experimental data were truncated at 1 μm because the larger particle sizes are irrelevant to this study.

Results for model A, in which the whole furnace was taken as the model reactor in which coagulation takes place, are shown in the second from the top panels. Here, coagulation commences at the particle concentration conditions denoted as state 2 (see Figure 1, with parameters T2, P2, V2, and C2, where T2 is the adiabatic flame temperature), as shown in Table 4. The gases then become more concentrated because of the temperature profile in the furnace, which causes decreases in specific volume of the flue gas (denoted as state 3, with parameters T3, P3, V3, and C3, where T3 is the temperature at sample point port 9). It should be noted that the actual measurements are made after double dilution under conditions of state 4 (with parameters T4, P4, V4, and C4, where T4 is the ambient temperature of about 300 K and V4 and C4 could be obtained from experimental data).

The parameters for model A predictions are shown in Table 4. Residence times in the furnace (from state 2 to state 3, t_{23}) of different cases varied as a result of the difference in the laminar-based gas flow rate. For the residence time in the sample probe (from state 3 to state 4, t_{34}), it was fixed at 0.25 s based on sample flow rates and the length of the sample probe.

The results from model A (Figure 3) show that, for all of the cases, none of predictions could come close to the experimental accumulation peak with model A. The experimental accumulation peak occurs between 0.22 and 0.38 μm, while the predicted result of model A is between 0.02 and 0.11 μm. As was noted above, this discrepancy could not be accounted for by an incorrect choice of nuclei size, because results were very insensitive to that parameter. Possibly coagulation alone might be an improper model (i.e., particle growth dominates), even though no additional condensation occurs in the sampling system. It is much more likely that the initial concentration of particles is grossly underestimated in model A because coagulation rates are very sensitive to that parameter.

Microscale mixing phenomena around individual particles is known to occur during volatile and char combustion.[17,18] Therefore, because much of the sub-micrometer particle composition consists of refractory species that were vaporized following a chemical reduction mechanism, it is reasonable to hypothesize that nucleation and coagulation occurs not so much in the mixed flue gas but rather in a concentrated region around each particle.

This line of thought led to model B, in which coagulation starts in a thin gas diffusion layer surrounding each particle. This would be more likely when the smallest pertinent fluid motion eddy size is large compared to the particle size. This configuration includes state 1 (see Figure 1, with parameters T1, P1, V1, and C1, where T1 and T2 are the adiabatic flame temperatures), followed by rapid mixing with the flue gas over the entire width of the furnace (state 2), followed by states 3 and 4 (to and in the sample probe), which are identical to those states in model A.

In comparison to state 2, state 1 has an extremely small control volume, which depends upon the diffusion layer thickness (δ). The ratio of the gas volume at state 2 after mixing with the flue gas (V2) to the gas volume at state 1 in the diffusion layer (V1) is defined as the dilution factor (η). Thus, the initial mass concentration of particles in model B is η times larger than that in model A. To simplify the calculation of

DOI: 10.1021/acs.energyfuels.7b03126
Energy Fuels 2018, 32, 4300−4307

Table 5. Initial Parameters for Accumulation Mode Prediction with Model B

accumulation mode with model B	Utah coal			PRB coal	
	OXY27	OXY70	air	OXY27	OXY50
initial temperature, T1 (K)	2000	2900	2000	2000	2600
diffusion layer thickness, δ (μm)	R^a	R	R	R	R
initial gas volume, V1 (m^3/h)	0.01863	0.01863	0.02648	0.02648	0.02648
initial mass concentration of particles, C1 (kg/m^3)	3.71×10^{-3}	2.48×10^{-2}	2.70×10^{-2}	1.38×10^{-2}	3.44×10^{-2}
residence time in the diffusion layer from state 1 to state 2, t_{12} (s)	0.05	0.05	0.05	0.05	0.05
predicted peak diameter (μm)	0.10	0.22	0.21	0.20	0.29
experimental peak diameter (μm)	0.30	0.22	0.24	0.38	0.29

[a] R is the radius of a single coal particle (μm).

Table 6. Initial Parameters for Nucleation Mode Prediction with Model A

nucleation mode with model A	Utah coal		PRB coal		
	OXY27	OXY70	air	OXY27	OXY50
total mass of vaporized ash for prediction (kg/h)	1.14×10^{-5}		5.73×10^{-5}	5.20×10^{-6}	6.15×10^{-4}
initial temperature, T2′ (K)	1600	1600	1600	1600	1600
initial gas volume, V2′ (m^3/h)	119.52	47.79	163.47	125.81	71.25
initial mass concentration of particles, C2′ (kg/m^3)	9.52×10^{-8}		3.51×10^{-7}	4.13×10^{-8}	8.63×10^{-6}
residence time in the furnace from state 2′ to state 3, $t_{2'3}$ (s)	4		6	8	13
predicted peak diameter (μm)	no peak		0.016	no peak	0.09
experimental peak diameter (μm)	0.04		0.06	0.07	0.09

diffusion layer volume, it is assumed that (1) all of the particles are in spherical shape and (2) the thickness of the diffusion layer surrounding a particle is equal to the radius of the particle ($\delta = R$).[30−32] With reasonable assumptions, the total diffusion layer volume of feed coal only depends upon the coal feed rate and its real density, regardless of the PSDs of coals. The residence time of coagulating particles in the diffusion layer was set at 0.05 s, which was thought to be a reasonable estimation based on the high flow rate of the primary coal jet in the flame.

The initial parameters for accumulation mode prediction with model B are listed in Table 5. It was noted that model B used the same parameters in states 2, 3, and 4 as well as the total mass of particles as model A.

In comparison to model A, the initial mass concentration of particles in model B increased by about 4 orders of magnitude. This was sufficient to obtain excellent agreement for the location of the accumulation peak for three of the five cases considered, as shown on the third panel down on the subgraphs in Figure 3. It was noted that, after entering state 2, that is, after mixing with the flue gas, the calculated PSD of the particles did not change significantly. This means that coagulation was essentially complete within the diffusion layer. Within reasonable limits, the residence time in the furnace was irrelevant.

For two of the five cases (Utah OXY27 and PRB OXY27), the predicted accumulation mode of model B still underestimated the accumulation mode peak diameter. For these two cases, it took diffusion layer thicknesses $\delta = 0.19R$ (Utah Sufco OXY27) and $\delta = 0.15R$ (PRB OXY27) to match the experimental data (see bottom panel on the subgraphs on Figure 3). Additional work is needed to understand why the OXY27 conditions lead to apparently thinner diffusion layers than for air or OXY70.

Overall, the comparison between predictions and measurements builds a strong case that microscale diffusion effects surrounding individual coal particles are important in determining the resulting PSD of the vaporized ash.

4.2. Nucleation Mode. A "nucleation" mode peak well below 0.1 μm was observed for the Utah Sufco OXY27 case, the PRB air case, the PRB OXY27 case (weak), and the PRB OXY50 case, as seen in Figure 2. PRB OXY50 showed nucleation mode particle concentrations that were significantly higher than those in the other two cases. The data[22] from scanning electron microscopy−energy-dispersive X-ray spectroscopy (SEM−EDS) analysis of size-segregated particles (see Table 7) showed that the particles of interest here were rich in sodium, and this was not the case for the same particle size range for runs in which flame temperatures were significantly higher. Sodium was more effectively scavenged by silicon particles at the higher temperatures. At lower temperatures, in the presence of sulfur, sodium sulfate was probably produced in the furnace and subsequently coagulated to contribute to the formation of the nucleation mode. On the basis of the experimental data analysis, the authors attempted to detect where the nucleation mode formed and whether this mode could be predicted with coagulation theory alone.

Thermodynamic equilibrium analysis using HSC Chemistry (6.0) software showed that various sodium-related species condensed at around 1600 K, a temperature that occurred between the flame zone and the sampling zone. All other possible vaporized species have condensed before reaching the sampling point (state 3, T3 listed in Table 4), indicating that nucleation occurs in the furnace and not in the probe, as previously hypothesized.[10]

On the basis of the HSC dew point predictions, an average of 1600 K was chosen for the initial coagulation temperature. Because coagulation of these species occurred in the furnace rather than in the flame zone, model A was applied for the prediction of the nucleation mode, with coagulation starting under particle concentration conditions denoted as state 2′ (between states 2 and 3, with parameters T2′, P2′, V2′, and C2′). Integration of the area under the nucleation mode in the experimental data yielded the total mass of vaporized ash aerosol contributing to this mode. Using a similar calculation method described above for predictions of the accumulation

DOI: 10.1021/acs.energyfuels.7b03126
Energy Fuels 2018, 32, 4300−4307

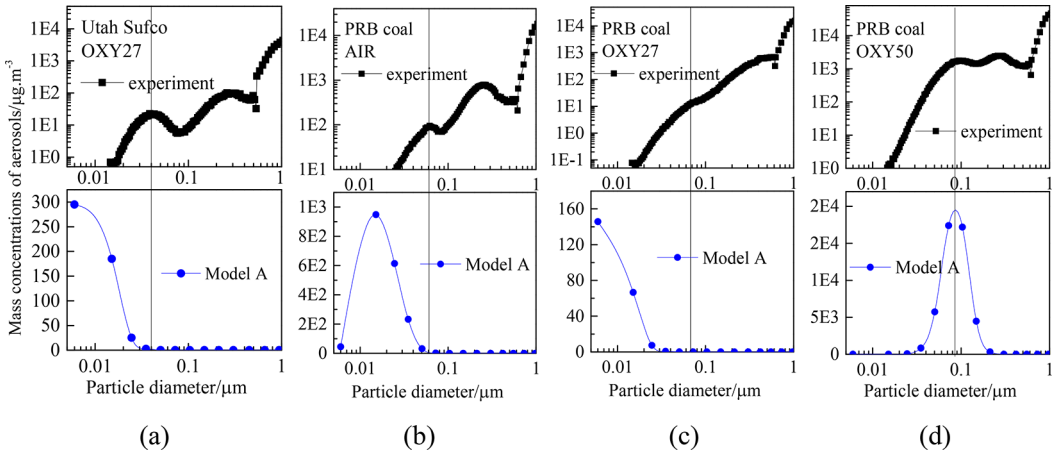

Figure 4. Comparison of predicted and experimental nucleation modes.

mode, the parameters for nucleation mode (model A) prediction are listed in Table 6.

The predicted nucleation modes were compared to experimental data, as shown in Figure 4.

It is seen in Figure 4 that, except for the PRB OXY50 case, where there was a high concentration of nuclei as model input, none of the other cases using a coagulation model alone could predict a nucleation mode close to the experimentally measured nucleation peak. There was no physical reason here to increase the particle concentration to the amount necessary to allow for the predicted coagulation peak to evolve to reach the experimental data. Therefore, it might be concluded that something other than coagulation, such as particle growth, may be the dominant mechanism, especially when the formation of sodium sulfate is considered.

To study the possible reasons accounting for the measured nucleation mode, typical elemental compositions of sampled ash aerosols were measured using SEM–EDS.[10] Those ash aerosols under 0.1 μm are shown in Table 7.[22]

It is found in Table 7 that sodium and sulfur account for considerable proportions in these particles under 0.1 μm, particularly in Utah Sufco coal, in which the ratio of sodium and sulfur is high, up to 16.98% and 12.29%, respectively, demonstrating the existence and coagulation of sodium sulfate inside the furnace to help to form the nucleation mode.

Table 7. Typical Elemental Compositions of Sampled Ash Aerosols (<0.1 μm)

		Utah coal			PRB coal	
	aerodynamic size (μm)	OXY27	OXY70	air	OXY27	OXY50
Na	0.0324	16.98	3.39	8.67	4.02	1.99
	0.0636	13.9	2.47	4.86	4.81	3.31
	0.0926	15.73	2.37	5.18	3.4	3.36
S	0.0324	12.29	6.69	9.53	8.43	9.21
	0.0636	14.93	8.01	11.94	10.09	9.46
	0.0926	17.67	8.38	12.5	9.5	9.97
Ca	0.0324	17.16	40.48	30.56	30.95	46.99
	0.0636	21	45.33	36.62	29.97	45.6
	0.0926	20.84	44.89	37.59	34.72	46.92
Si	0.0324	16.16	24.55	9.94	16.45	16.5
	0.0636	16.62	26.64	10.05	15.1	16.49
	0.0926	13.91	27.28	8.97	13.31	15.51
P	0.0324			1.84	2.59	2.67
	0.0636			2.49	4.15	6.08
	0.0926			2.88	3.76	6.71

In comparison to low inlet oxygen cases (Utah Sufco and PRB at OXY27), the high inlet oxygen cases (Utah Sufco OXY70 and PRB OXY50) tend to have less sodium and sulfur in <0.1 μm particles and more calcium and silicon (see Table 7). The main explanation for this phenomenon is that a higher inlet oxygen concentration increased the adiabatic flame temperature; thus, more vaporized sodium was scavenged by aluminosilicates and passed into fragmentation mode (>1 μm), despite more sodium being vaporized, and this led to less sodium in ash.[33,34] Sulfur was decreased at the same time as a result of the lower amounts of sodium with which to react.[35] This could be used to explain the disappearance of the nucleation mode in the Utah Sufco OXY70 case (see Figure 2), in which a sharp decrease of the sodium and sulfur amounts in <0.1 μm ash particles was observed in comparison to values for the OXY27 condition.

In contrast to the foregoing, there is good agreement between the data and coagulation theory for the PRB OXY50 condition (see Figure 4), even though the sodium concentration in <0.1 μm ash is low (~1.99%). These particles are no longer a sodium fume but consist largely of calcium (see Table 7). The particle concentration in the flue gas is high (Figure 4), and this allows for the "nucleation" mode at 0.09 μm to be predicted (see Figure 4) using model A, namely, assuming true nucleation at 1600 K, as with the other cases, and subsequent coagulation in the mixed flue gas. Therefore, calcium species, presumably, coagulate to form this nucleation mode. Moreover, in comparison to the significant decrease in Utah Sufco coal of sulfur in the smallest particles when going from OXY27 to OXY70, there was no obvious change in the amount of sulfur in the same sized particles in going from PRB OXY27 to PRB OXY50. This indicates that sulfur in PRB coal was more likely to react with calcium, probably in the form of calcium sulfate, and calcium may not be scavenged like sodium at the high temperatures. In addition, the content of phosphorus in PRB coal increased with higher temperatures, and it was found to be as high as 7% in the PRB OXY50 case.[22] Phosphorus might also combine with calcium to generate calcium phosphate for coagulation, the effect of which could not be ignored. Overall, the purported "nucleation" mode in PRB OXY50 is consistent with coagulation occurring within high concentrations of particles containing calcium species, including calcium sulfate

DOI: 10.1021/acs.energyfuels.7b03126
Energy Fuels 2018, 32, 4300–4307

and calcium phosphorus. In contrast, the nucleation modes in the other cases were formed from the original nuclei by a mechanism other than coagulation, most likely by particle growth, leading to sodium sulfate particles.

In conclusion, it is found that coagulation behavior that contributes to the so-called "nucleation" mode occurs in the furnace rather than inside the probe, as assumed in previous hypotheses.[10] Coagulation alone could not account for the nucleation mode for all but one of the cases, suggesting that particle growth plays a dominant role in forming the nucleation mode. The exception to this was when the "fume" consisted of many small particles containing calcium.

5. CONCLUSION

The most important conclusion from this work is that predictions of the vaporized ash PSD must account for microscale diffusion phenomena near individual coal and coal char particles, where most of the coagulation takes place. This work also showed that modeling aerosol dynamics can be used to provide insight into some of the finer details of how a coal particle burns and forms particles from vaporized ash constituents. Agreement between predictions of the accumulation mode and experimental data was good, provided that the nuclei from vaporized minerals had 0.05 s to coagulate within a diffusion layer surrounding each particle.

A comparison between predictions based on coagulation and experimental data on the so-called "nucleation" mode at <0.07 μm was poor and suggested that coagulation could not account for all but one of the nucleation modes experimentally observed. For many runs, the particles within this mode consisted of sodium sulfate, where particle growth might be the dominant mechanism determining the resultant PSD. In the one run where coagulation did fit the experimental data, that process was promoted by large concentrations of particles containing calcium, sulfur, and phosphorus.

Clearly, future work should include particle growth mechanisms as well as coagulation. Coagulation alone, however, can clearly explain the dominant accumulation sub-micrometer mode at around 0.3 μm.

■ ASSOCIATED CONTENT

Supporting Information

The Supporting Information is available free of charge on the ACS Publications website at DOI: 10.1021/acs.energyfuels.7b03126.

Detailed input parameters of MAEROS used to predict the accumulation mode of five cases (Tables S1–S5) and nucleation mode input (no nucleation mode occurred for Utah Sufco OXY70) (Tables S6–S9) (PDF)

■ AUTHOR INFORMATION

Corresponding Author

*E-mail: jost.wendt@utah.edu.

ORCID

Jost O. L. Wendt: 0000-0002-0104-0763

Notes

The authors declare no competing financial interest.

■ ACKNOWLEDGMENTS

The authors acknowledge financial assistance from the U.S. National Science Foundation (Award 1603249), and Huimin Liu is grateful for financial support from the China Scholarship Council (CSC). The authors also acknowledge Fred Gelbard for providing the MAEROS2 code that was used here.

■ REFERENCES

(1) Yao, Q.; Li, S.-Q.; Xu, H.-W.; Zhuo, J.-K.; Song, Q. Reprint of: studies on formation and control of combustion particulate matter in China: A review. *Energy* **2010**, *35* (11), 4480–4493.

(2) Helble, J. A model for the air emissions of trace metallic elements from coal combustors equipped with electrostatic precipitators. *Fuel Process. Technol.* **2000**, *63* (2), 125–147.

(3) Zhuang, Y.; Pavlish, J. H. Fate of hazardous air pollutants in oxygen-fired coal combustion with different flue gas recycling. *Environ. Sci. Technol.* **2012**, *46* (8), 4657–4665.

(4) Shah, P.; Strezov, V.; Prince, K.; Nelson, P. F. Speciation of As, Cr, Se and Hg under coal fired power station conditions. *Fuel* **2008**, *87* (10–11), 1859–1869.

(5) Hower, J. C.; Senior, C. L.; Suuberg, E. M.; Hurt, R. H.; Wilcox, J. L.; Olson, E. S. Mercury capture by native fly ash carbons in coal-fired power plants. *Prog. Energy Combust. Sci.* **2010**, *36* (4), 510–529.

(6) Helble, J.; Sarofim, A. F. Influence of char fragmentation on ash particle size distributions. *Combust. Flame* **1989**, *76* (2), 183–196.

(7) Gao, Q.; Li, S.; Yuan, Y.; Zhang, Y.; Yao, Q. Ultrafine particulate matter formation in the early stage of pulverized coal combustion of high-sodium lignite. *Fuel* **2015**, *158*, 224–231.

(8) Linak, W. P.; Yoo, J.-I.; Wasson, S. J.; Zhu, W.; Wendt, J. O. L.; Huggins, F. E.; et al. Ultrafine ash aerosols from coal combustion: Characterization and health effects. *Proc. Combust. Inst.* **2007**, *31* (2), 1929–1937.

(9) Wu, H.; Pedersen, A. J.; Glarborg, P.; Frandsen, F. J.; Dam-Johansen, K.; Sander, B. Formation of fine particles in co-combustion of coal and solid recovered fuel in a pulverized coal-fired power station. *Proc. Combust. Inst.* **2011**, *33* (2), 2845–2852.

(10) Zhan, Z.; Fry, A.; Zhang, Y.; Wendt, J. O. L. Ash aerosol formation from oxy-coal combustion and its relation to ash deposit chemistry. *Proc. Combust. Inst.* **2015**, *35* (2), 2373–2380.

(11) Linak, W. P.; Wendt, J. O. L. Trace metal transformation mechanisms during coal combustion. *Fuel Process. Technol.* **1994**, *39* (1), 173–198.

(12) McElroy, M.; Carr, R.; Ensor, D.; Markowski, G. Size distribution of fine particles from coal combustion. *Science* **1982**, *215* (4528), 13–19.

(13) Damle, A. S.; Ensor, D. S.; Ranade, M. B. Coal Combustion Aerosol Formation Mechanisms: A Review. *Aerosol Sci. Technol.* **1981**, *1* (1), 119–133.

(14) Jia, Y.; Lighty, J. S. Ash particulate formation from pulverized coal under oxy-fuel combustion conditions. *Environ. Sci. Technol.* **2012**, *46* (9), 5214–5221.

(15) Neville, M.; Quann, R.; Haynes, B.; Sarofim, A. F. Vaporization and condensation of mineral matter during pulverized coal combustion. *Symp. (Int.) Combust., [Proc.]* **1981**, *18*, 1267–1274.

(16) Quann, R.; Sarofim, A. F. Vaporization of refractory oxides during pulverized coal combustion. *Symp. (Int.) Combust., [Proc.]* **1982**, *19*, 1429–1440.

(17) Wendt, J. O. L. Fundamental coal combustion mechanisms and pollutant formation in furnaces. *Prog. Energy Combust. Sci.* **1980**, *6* (2), 201–222.

(18) Hecht, E. S.; Shaddix, C. R.; Geier, M.; Molina, A.; Haynes, B. S. Effect of CO2 and steam gasification reactions on the oxy-combustion of pulverized coal char. *Combust. Flame* **2012**, *159* (11), 3437–3447.

(19) Hecht, E. S.; Shaddix, C. R.; Molina, A.; Haynes, B. S. Effect of CO2 gasification reaction on oxy-combustion of pulverized coal char. *Proc. Combust. Inst.* **2011**, *33* (2), 1699–1706.

(20) Molina, A.; Sarofim, A. F.; Ren, W.; Lu, J.; Yue, G.; Beér, J. M.; et al. Effect of boundary layer reactions on the conversion of char-N to NO, N_2O, and HCN at fluidized-bed combustion conditions. *Combust. Sci. Technol.* **2002**, *174* (11–12), 43–71.

DOI: 10.1021/acs.energyfuels.7b03126
Energy Fuels 2018, 32, 4300–4307

(21) Zhan, Z.; Bool, L. E.; Fry, A.; Fan, W.; Xu, M.; Yu, D.; et al. Novel Temperature-Controlled Ash Deposition Probe System and Its Application to Oxy-coal Combustion with 50% Inlet O2. *Energy Fuels* **2014**, *28* (1), 146−154.
(22) Davis, K. A.; Chiodo, A. P. *Research Performance Progress Report: Characterizing Impacts of High Temperatures and Pressures in Oxy-Coal Combustion Systems*; Reaction Engineering International: Murray, UT, 2016; pp 10−31, DE-FE0025168.
(23) Gelbard, F. *MAEROS User Manual*. Sandia National Laboratories: Albuquerque, NM, 1982; NUREG/CR-1391, SAND80-0822, http://prod.sandia.gov/techlib/access-control.cgi/1980/800822.pdf.
(24) Gelbard, F.; Seinfeld, J. H. Simulation of multicomponent aerosol dynamics. *J. Colloid Interface Sci.* **1980**, *78* (2), 485−501.
(25) Gelbard, F.; Fitzgerald, J. W.; Hoppel, W. A. A one-dimensional sectional model to simulate multicomponent aerosol dynamics in the marine boundary layer: 3. Numerical methods and comparisons with exact solutions. *J. Geophys. Res.* **1998**, *103* (D13), 16119−16132.
(26) Davis, S. B.; Gale, T. K.; Wendt, J. O. L.; Linak, W. P. Multicomponent coagulation and condensation of toxic metals in combustors. *Symp. (Int.) Combust., [Proc.]* **1998**, *27*, 1785−1791.
(27) Linak, W. P.; Miller, C. A.; Wendt, J. O. L. Fine particle emissions from residual fuel oil combustion: Characterization and mechanisms of formation. *Proc. Combust. Inst.* **2000**, *28* (2), 2651−2658.
(28) Jöller, M.; Brunner, T.; Obernberger, I. Modeling of aerosol formation during biomass combustion for various furnace and boiler types. *Fuel Process. Technol.* **2007**, *88* (11−12), 1136−1147.
(29) Beketov, A.; Sorokin, A.; Alipchenkov, V.; Mosunova, N. Comparison of different methods used in integral codes to model coagulation of aerosols. *Therm. Eng.* **2013**, *60* (9), 647−652.
(30) Caram, H. S.; Amundson, N. R. Diffusion and reaction in a stagnant boundary layer about a carbon particle. *Ind. Eng. Chem. Fundam.* **1977**, *16* (2), 171−181.
(31) Mon, E.; Amundson, N. R. Diffusion and reaction in a stagnant boundary layer about a carbon particle. 2. An extension. *Ind. Eng. Chem. Fundam.* **1978**, *17* (4), 313−321.
(32) Sotirchos, S.; Amundson, N. R. Dynamic behavior of a porous char particle burning in an oxygen-containing environment: Part I: Constant particle radius. *AIChE J.* **1984**, *30* (4), 537−549.
(33) Gallagher, N. B.; Bool, L. E.; Wendt, J. O. L.; Peterson, T. W. Alkali metal partitioning in Ash from pulverized coal combustion. *Combust. Sci. Technol.* **1990**, *74* (1−6), 211−221.
(34) Gallagher, N. B.; Peterson, T. W.; Wendt, J. O. L. Sodium partitioning in a pulverzed coal combustion environment. *Symp. (Int.) Combust., [Proc.]* **1996**, *26* (2), 3197−3204.
(35) Raask, E. *Mineral Impurities in Coal Combustion—Behaviour, Problems and Remedial Measures*; Hemisphere Publishing Corporation: Washington, D.C., 1985.

DOI: 10.1021/acs.energyfuels.7b03126
Energy Fuels 2018, 32, 4300−4307